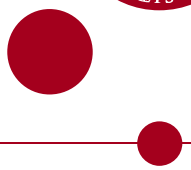

Bachelor project

Oliver Ovsée Laub Solow

Caroli-de Gennes-Matricon states in the vortex cores of unconventional superconductors

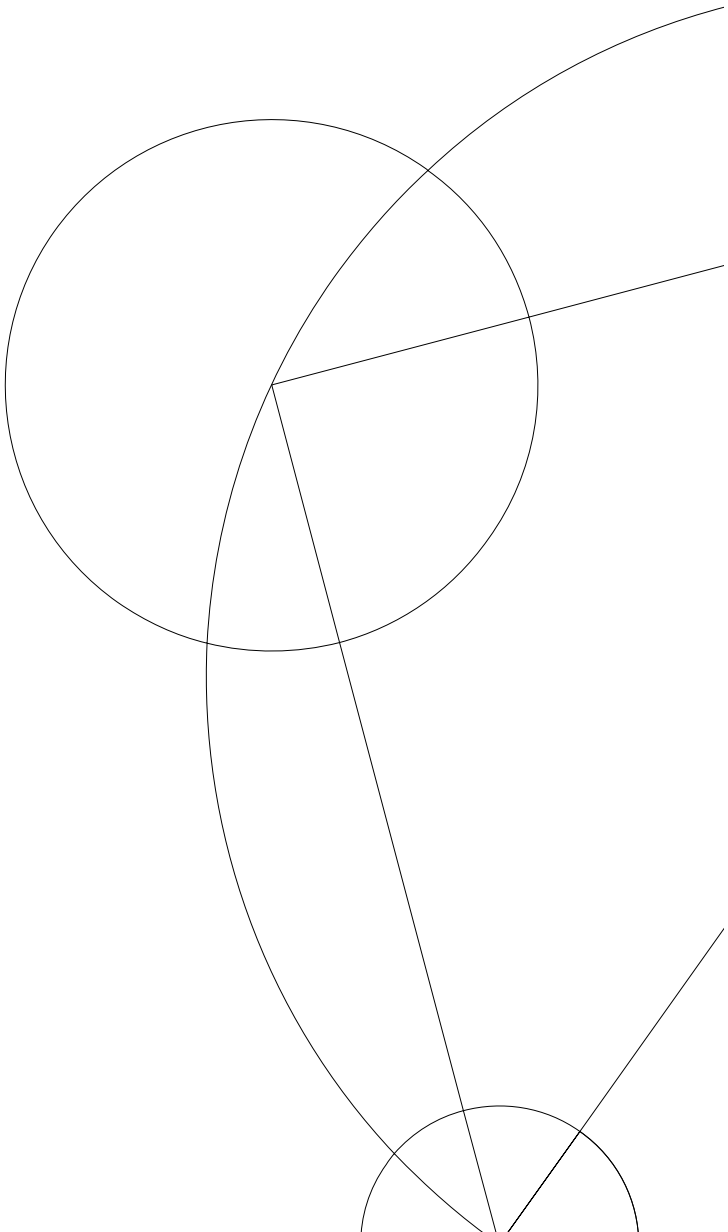

Supervisor: Brian Møller Andersen

Handed in June 16 2021

Abstract

In this thesis, we will analyze the sub-gap states that arise when a vortex forms around a magnetic impurity in a type II superconductor. To do this, we will first study the theory of superconductivity, and use this to derive the Bogoliubov-de Gennes equations, which describes a superconductor with spatial inhomogeneity. We then use the symmetries of a vortex to write these equations in terms of Bessel functions, allowing the equations to be solved numerically. We solve these equations numerically, first for well-understood cases with no magnetic impurities, and then for the case of a magnetic impurity. This is primarily used to confirm that our program for solving these equations works. Finally, we consider self-consistent solutions for the case of a helical band on the surface of the superconductor and find that the surface states look the same whether the superconducting gap is generated in the surface or induced by the bulk superconductor.

Contents

1 Introduction

Superconductivity is one of the most fascinating topics in condensed matter physics. Ever since it was discovered by Onnes in the early 20th century, physicists have tried to get a better understanding of how superconductivity occurs. With the advent of BCS theory in the 1950s, we have a theory that explains a lot of superconductors completely, and which forms a framework for understanding the behaviour of all superconductors.
In this thesis, we will be using BCS theory to investigate the vortices that form when a superconductor is exposed to a magnetic field. We will be investigating whether magnetic impurities can serve the role of a magnetic field and form a vortex, and we will be invetstigating the nature of vortices in materials and situations where superconductivity coexists with topological surface states. This analysis will be used to make predictions about what an electron microscopy experiment might observe in the analyzed cases.

2 Theory

2.1 Second quantization[1]

Throughout the thesis, we will be using the formalism of second quantization. In this formalism, we have two operators a_m and $a_m^\dagger$, which are said to annihilate and create, respectively, a particle with quantum number m. This is seen by applying these operators to a quantum state:

$$a_m^\dagger |0\rangle = |0, 0, ..., 0, 1, 0, ...\rangle \tag{1}$$

Where $|0\rangle$ is the vacuum state with no particles and $|0, 0, ..., 0, 1, 0, ...\rangle$ is the state with one particle with quantum number m. In general, we write a state as $|n_1, n_2, n_3, ...\rangle$ where n_m is the number of particles with a given quantum number.
In this thesis, we will only be using fermion operators. This means that the operators follows the following rules:

$$a_m |0\rangle = 0, a_m^\dagger \ \ |0, 0, ..., 0, 1, 0, ...\rangle = 0 \tag{2}$$

In other words, applying an annihilation operator to a state with no particles gives zero, and so does applying a creation operator to a state which is already occupied, since two fermions cannot be in the same state. From these rules, we can derive a set of anticommutator relations:

$$\begin{aligned} \{a_m, a_n\} = \{a_m^\dagger, a_n^\dagger\} = 0 \\ \{a_m, a_n^\dagger\} = \delta_{m,n} \end{aligned} \tag{3}$$

Where the anticommutator is defined as $\{A, B\} = AB + BA$. We can use these creation and annihilation operators to define a range of other operators. The most important one is the number operator $n_m = a_m^\dagger a_m$, which counts the number of particle in the quantum state m. Since we are working with fermions, we know the expectation value of the number operator: $\langle n_m \rangle = f(E_m)$ where $f(E)$ is the Fermi-Dirac function:

$$f(E) = \frac{1}{e^{\frac{E-\varepsilon_F}{kT}} + 1} \tag{4}$$

[1] This section is based on [1]

2.2 BCS theory[2]

BCS theory is a microscopic theory which describes many superconductors. In this theory, superconductivity comes about due to the formation of Cooper pairs, which are pairs of electrons. Specifically, BCS theory uses an s-wave pairing between a spin-up electron with momentum $\boldsymbol{k}$ and a spin-down electron with momentum $-\boldsymbol{k}$. This pairing happens near the Fermi surface of the superconductor. Specifically, since the pairing is mediated by phonons, it happens at energies between $E_F - \hbar\omega_D$ and $E_F + \hbar\omega_D$ where ω_D is the Debye frequency. This yields the following Hamiltonian [1]:

$$H_{BCS} = \sum_{\boldsymbol{k}\sigma} \xi_{\boldsymbol{k}} c^\dagger_{\boldsymbol{k}\sigma} c_{\boldsymbol{k}\sigma} - \frac{g}{2} \sum_{\boldsymbol{k},\boldsymbol{k}'} c^\dagger_{\boldsymbol{k}\uparrow} c^\dagger_{-\boldsymbol{k}\downarrow} c_{-\boldsymbol{k}'\downarrow} c_{\boldsymbol{k}'\uparrow} \tag{5}$$

Where $\xi_{\boldsymbol{k}} = \frac{\hbar^2 \boldsymbol{k}^2}{2m^*} - E_F$ is the kinetic energy of an electron with momentum $\boldsymbol{k}$, measured from the Fermi energy. This Hamiltonian consists of a kinetic part and a part that governs the interaction of Cooper pairs, which allows one Cooper pair to scatter into another. Due to the final term, this Hamiltonian cannot be solved analytically for any interesting situation. To solve it, we need to perform a mean-field decoupling:

$$c^\dagger_{\boldsymbol{k}\uparrow} c^\dagger_{-\boldsymbol{k}\downarrow} c_{-\boldsymbol{k}'\downarrow} c_{\boldsymbol{k}'\uparrow} \approx -\langle c^\dagger_{\boldsymbol{k}\uparrow} c^\dagger_{-\boldsymbol{k}\downarrow}\rangle \langle c_{-\boldsymbol{k}'\downarrow} c_{\boldsymbol{k}'\uparrow}\rangle + \langle c^\dagger_{\boldsymbol{k}\uparrow} c^\dagger_{-\boldsymbol{k}\downarrow}\rangle c_{-\boldsymbol{k}'\downarrow} c_{\boldsymbol{k}'\uparrow} + c^\dagger_{\boldsymbol{k}\uparrow} c^\dagger_{-\boldsymbol{k}\downarrow} \langle c_{-\boldsymbol{k}'\downarrow} c_{\boldsymbol{k}'\uparrow}\rangle$$

This allows us to define a new quantity, the *superconducting gap*:

$$\Delta = \frac{g}{2} \sum_{\boldsymbol{k}} \langle c_{-\boldsymbol{k}\downarrow} c_{\boldsymbol{k}\uparrow}\rangle \tag{6}$$

We can write the mean field BCS Hamiltonian in terms of this superconducting gap, ignoring the constant term since it doesn't change the dynamics of the system.

$$H_{BCS} = \sum_{\boldsymbol{k}\sigma} \xi_{\boldsymbol{k}} c^\dagger_{\boldsymbol{k}\sigma} c_{\boldsymbol{k}\sigma} - \sum_{\boldsymbol{k}} \left(\Delta c^\dagger_{\boldsymbol{k}\uparrow} c^\dagger_{-\boldsymbol{k}\downarrow} + \Delta^* c_{-\boldsymbol{k}\downarrow} c_{\boldsymbol{k}\uparrow} \right) \tag{7}$$

This Hamiltonian can be written as a matrix:

$$H_{BCS} = \sum_{\boldsymbol{k}} \begin{pmatrix} c^\dagger_{\boldsymbol{k}\uparrow} & c_{-\boldsymbol{k}\downarrow} \end{pmatrix} \begin{pmatrix} \xi_{\boldsymbol{k}} & -\Delta \\ -\Delta^* & -\xi_{\boldsymbol{k}} \end{pmatrix} \begin{pmatrix} c_{\boldsymbol{k}\uparrow} \\ c^\dagger_{-\boldsymbol{k}\downarrow} \end{pmatrix} \tag{8}$$

To diagonalize this, we perform a unitary transformation:

$$\begin{pmatrix} \gamma_{\boldsymbol{k}\uparrow} \\ \gamma^\dagger_{-\boldsymbol{k}\downarrow} \end{pmatrix} = U \begin{pmatrix} c_{\boldsymbol{k}\uparrow} \\ c^\dagger_{-\boldsymbol{k}\downarrow} \end{pmatrix} = \begin{pmatrix} u_{\boldsymbol{k}} & v^*_{\boldsymbol{k}} \\ -v_{\boldsymbol{k}} & u^*_{\boldsymbol{k}} \end{pmatrix} \begin{pmatrix} c_{\boldsymbol{k}\uparrow} \\ c^\dagger_{-\boldsymbol{k}\downarrow} \end{pmatrix} \tag{9}$$

Which is equivalent to saying:

$$\begin{aligned} c^\dagger_{\boldsymbol{k}\uparrow} &= u^*_{\boldsymbol{k}} \gamma^\dagger_{\boldsymbol{k}\uparrow} + v_{\boldsymbol{k}} \gamma_{-\boldsymbol{k}\downarrow} \\ c^\dagger_{-\boldsymbol{k}\downarrow} &= u^*_{\boldsymbol{k}} \gamma^\dagger_{-\boldsymbol{k}\downarrow} - v_{\boldsymbol{k}} \gamma_{\boldsymbol{k}\uparrow} \end{aligned} \tag{10}$$

We then demand that these operators diagonalize the Hamiltonian:

$$H_{BCS} = \sum_{\boldsymbol{k}} E_{\boldsymbol{k}} \gamma^\dagger_{\boldsymbol{k}\sigma} \gamma_{\boldsymbol{k}\sigma}$$

Clearly, $\pm E_{\boldsymbol{k}}$ is the eigenvalue of the Hamiltonian. However, we know what the Hamiltonian looks like, and some basic linear algebra tells us that these eigenvalues must be

$$E_k = \sqrt{\xi^2_{\boldsymbol{k}} + |\Delta|^2} \tag{11}$$

[2]This section is based on [2].

This shows why we describe Δ as the gap, since it's the minimum positive/maximum negative eigenenergy of the system. We can intrepret this energy as the energy of a new quasiparticle which is created and annihilated by $\gamma^\dagger$ and γ respectively. This quasiparticle is the so-called bogoliubon. These quasiparticles are superpositions of a hole and an electron, with $|u_k|^2$ being the probability of measuring an electron and $|v_k|^2$ being the probability of measuring a hole. Since these quasiparticles are fermions, they follow the fermion anticommutator relations:

$$\{\gamma^\dagger_{\boldsymbol{k}\sigma}, \gamma_{\boldsymbol{k}'\sigma'}\} = \delta_{\boldsymbol{k}\boldsymbol{k}'}\delta_{\sigma\sigma'}, \{\gamma_{\boldsymbol{k}\sigma}, \gamma_{\boldsymbol{k}'\sigma'}\} = 0 \tag{12}$$

We can now insert our new operators into the definition of Δ to find that:

$$\Delta = \frac{g}{2}\sum_{\boldsymbol{k}}\langle c_{-\boldsymbol{k}\downarrow}c_{\boldsymbol{k}\uparrow}\rangle = \frac{g}{2}\sum_{\boldsymbol{k}}\langle(u_{\boldsymbol{k}}\gamma_{-\boldsymbol{k}\downarrow} - v^*_{\boldsymbol{k}}\gamma^\dagger_{\boldsymbol{k}\uparrow})(u_{\boldsymbol{k}}\gamma_{\boldsymbol{k}\uparrow} + v^*_{\boldsymbol{k}}\gamma^\dagger_{-\boldsymbol{k}\downarrow})\rangle = \frac{g}{2}\sum_{\boldsymbol{k}} u_{\boldsymbol{k}}v^*_{\boldsymbol{k}}(1 - 2f(E_{\boldsymbol{k}})) \tag{13}$$

Where we used the anticommutator relations, as well as the fact $\langle\gamma_{\boldsymbol{k}\sigma}\gamma^\dagger_{\boldsymbol{k}\sigma}\rangle = f(E_{\boldsymbol{k}})$ where $f(E_{\boldsymbol{k}})$ is the Fermi-Dirac function.

2.3 Bogoliubov-de Gennes equations[3]

We now want to consider the case where there is spatial variation in our system. In this case, the BCS mean field Hamiltonian is:

$$\begin{aligned} H_{BCS} = &\int \mathrm{d}\boldsymbol{r}\sum_\sigma \psi^\dagger_\sigma(\boldsymbol{r})H_e(\boldsymbol{r})\psi_\sigma(\boldsymbol{r}) \\ &+\Delta(\boldsymbol{r})\psi^\dagger_\uparrow(\boldsymbol{r})\psi^\dagger_\downarrow(\boldsymbol{r}) + \Delta^*(\boldsymbol{r})\psi_\downarrow(\boldsymbol{r})_\uparrow(\boldsymbol{r}) \end{aligned} \tag{14}$$

Where $\psi_\sigma(\boldsymbol{r})^\dagger$ and $\psi_\sigma(\boldsymbol{r})$ are the creation and annihilation operators respectively for an electron with spin σ at position $\boldsymbol{r}$, and H_e is the Hamiltonian for the uncoupled electrons, in the simplest case:

$$H_e = -\frac{1}{2m^*}(\nabla - ie\boldsymbol{A})^2 \tag{15}$$

Where the minus sign is to ensure comparability with the results from [3], and corresponds to looking at a hole-like band, rather than an electron-like band. Similarly to when there is no spatial variation, we solve this by introducing new operators. This time, however, $\mathbf{k}$ isn't guaranteed to be a good quantum number, so we use generic quantum numbers n and sum over all n:

$$\begin{aligned} \psi^\dagger_\uparrow &= \sum_n u^*_{n\uparrow}(\boldsymbol{r})\gamma^\dagger_{n\uparrow} + v_{n\uparrow}(\boldsymbol{r})\gamma_{n\downarrow} \\ \psi^\dagger_\downarrow &= \sum_n u^*_{n\downarrow}(\boldsymbol{r})\gamma^\dagger_{n\downarrow} - v_{n\downarrow}(\boldsymbol{r})\gamma_{n\uparrow} \end{aligned} \tag{16}$$

We then demand that these new operators diagonalize the Hamiltonian:

$$H_{BCS} = E_0 + \sum_{n\sigma} E_n\gamma^\dagger_{n\sigma}\gamma_{n\sigma} \tag{17}$$

The E_0 term turns out to be negligible in our case, and can be thrown away[9]. We can now compare these two expressions of the Hamiltonian. We do this by comparing the commutator of the Hamiltonian with ψ and γ, using the rule that $[AB, C] = A\{B, C\} - \{A, C\}B$:

$$[H_{BCS}, \gamma_{n\sigma}] = E_n\gamma_{n\sigma} \tag{18}$$

[3]This section is based on [1]

$$[H_{BCS}, \psi_\uparrow] = H_e\psi_\uparrow - \Delta\psi_\downarrow^\dagger \tag{19}$$

We now insert equations (16) and (18) into (19):

$$[H_{BCS}, \psi_\uparrow] = [H_{BCS}, \sum_n u_{n\uparrow}(\boldsymbol{r})\gamma_{n\uparrow} + v_{n\uparrow}^*(\boldsymbol{r})\gamma_{n\downarrow}^\dagger] = E_n \sum_n u_{n\uparrow}(\boldsymbol{r})\gamma_{n\uparrow} + v_{n\uparrow}^*(\boldsymbol{r})\gamma_{n\downarrow}^\dagger$$

$$[H_{BCS}, \psi_\uparrow] = H_e\psi_\uparrow - \Delta\psi_\downarrow^\dagger = H_e \sum_n u_{n\uparrow}(\boldsymbol{r})\gamma_{n\uparrow} + v_{n\uparrow}^*(\boldsymbol{r})\gamma_{n\downarrow}^\dagger - \Delta \sum_n u_{n\downarrow}^*(\boldsymbol{r})\gamma_{n\downarrow}^\dagger - v_{n\downarrow}(\boldsymbol{r})\gamma_{n\uparrow} \tag{20}$$

We can now set all the terms with the same γ operator equal to each other. This gives us two new equations:

$$\begin{aligned} H_e u_{n\uparrow} + \Delta v_{n\downarrow} &= E_n u_{n\uparrow} \\ H_e v_{n\uparrow}^* - \Delta u_{n\downarrow}^* &= E_n v_{n\uparrow}^* \end{aligned} \tag{21}$$

We can do the same thing with $\psi_\downarrow$ to get two more equations, and then combine all four equations. We define a spinor $\boldsymbol{\Phi}_n(\boldsymbol{r}) = (u_{n\uparrow}(\boldsymbol{r}), u_{n\downarrow}(\boldsymbol{r}), v_{n\downarrow}(\boldsymbol{r}), -v_{n\uparrow}(\boldsymbol{r}))^T$ in accordance with [8]. We can write our four equations as a single matrix equation:

$$\begin{pmatrix} H_e & 0 & \Delta & 0 \\ 0 & H_e & 0 & \Delta \\ \Delta^* & 0 & -H_e & 0 \\ 0 & \Delta^* & 0 & -H_e \end{pmatrix} \boldsymbol{\Phi}_n = E_n \boldsymbol{\Phi}_n \tag{22}$$

These are the *Bogoliubov-de Gennes equations* (BdG equations), which will form the basis of our further calculations.

Since we now distinguish between spin up and spin down, we also need to consider the gap function. For the inhomogeneous case, the gap can be written as $\Delta(\boldsymbol{r}) = \frac{g}{2}\langle\psi_\downarrow(\boldsymbol{r})\psi_\uparrow(\boldsymbol{r})\rangle$. We can then insert (16) into this definition to get:

$$\Delta(\boldsymbol{r}) = \frac{g}{2}\sum_n \left(u_{n\uparrow}(\boldsymbol{r})v_{n\downarrow}^*(\boldsymbol{r})f(E_n) - u_{n\downarrow}(\boldsymbol{r})v_{n\uparrow}^*(\boldsymbol{r})(1-f(E_n))\right) \tag{23}$$

Where $f(E_n)$ is the Fermi-Dirac function.

The Bogoliubov-de Gennes equation as defined here assumes that the free electron Hamiltonian has no spin-coupling parts. This is the case for the parabolic Hamiltonian which describes free electrons inside the bulk of our superconductor, but as we will see later, this doesn't necessarily apply to the surface.

2.4 Sub-gap states

One of the ways of classifying superconductors is by type. A superconductor can either be type I or type II. A type I superconductor will, when exposed to a large magnetic field, lose all superconductivity at once. A type II superconductor, on the other hand, will form vortices which captures the magnetic flux lines and shields the rest of the superconductor from the magnetic field, which can otherwise break the Cooper pairs. These vortices are a great example of an inhomogeneity that we can study with the BdG equations. It turns out that in such a vortex, not all of the states are pushed out of the gap that forms in a superconductor. Those that don't get pushed out are the so-called *Caroli-de Gennes-Matricon*(CdGM) states. The CdGM states are localized around the vortex core, where Δ is small and thus states with sub-gap energy is possible. The CdGM states closest to the Fermi level have an energy distribution that is roughly $l\frac{\Delta^2}{\varepsilon_F}$ [4][6], where l is the angular momentum, assuming that we're in the clean limit where $\Delta \ll \varepsilon_F$. As such, a state with $l = 0$ would have zero energy. These zero-energy CdGM states turn out to be important, and will be covered in

more detail later. Another type of sub-gap state is the Yu-Shiba-Rusinov (YSR) state, which is formed when there is a magnetic impurity in a superconductor. One of the things we will be observing is how these YSR states differ from the CdGM states formed by a vortex.
These sub-gap states can be directly measured by electron microscopy. An electron microscope measures the current between the sample and the tip of the microscope for various voltages. This current is directly proportional to the local density of states. The density of states (DOS) is the number of states at a given energy. The *local* density of states is the number of states at a given energy, times the probability of each state at a given position. In other words[11]:

$$N_\sigma(V,r) = \sum_n (|u_{n\sigma}(\boldsymbol{r})|^2 \delta(E-V) + |v_{n\sigma}(\boldsymbol{r})|^2 \delta(E+V)) \tag{24}$$

This gives the local density of states for a given spin, the total local density of states is just the sum over spins. When actually measuring, the delta functions are replaced by the derivative of the Fermi-Dirac function $f'(E \pm V)$. With this equation, we can simulate what an electron microscope would measure, which is how we actually measure things like the superconducting gap. As such, this allows us to translate our theory into concrete predictions about what a system behaves like.

2.5 Magnetization

We're interested in exploring what happens when a magnetic impurity is placed either inside or on the surface of a superconductor. To do this we have to look at how such an impurity interacts with the surrounding electrons. We follow the model of [3] and consider two types of interaction: an exchange interaction $H_{ex} = -J(r)\mathbf{I}\cdot\mathbf{J}$ where $\mathbf{I}$ is the magnetic moment of the impurity, $\mathbf{J}$ is the total angular momentum of the electron, and $J(r)$ is a function that determines the range and strength of the interaction. We also consider a spin-orbit coupling: $H_{SOC} = -\lambda_{so}(r)\boldsymbol{L}\cdot\boldsymbol{\sigma}$, which we take as the Elliott-Yafet coupling induced by the impurity in our enviroment, which already has a strong spin-orbit coupling [3].
To simplify the calculations somewhat, we make some simple assumptions. The first one is that the impurity magnetic moment is perpendicular to the surface we're considering: $\mathbf{I} = M\hat{z}$. Next, we assume that both $J(r)$ and $\lambda_{so}(r)$ are simple exponentially decaying functions, and furthermore that they both have the same decay length r_0. We can thus write these impurity Hamiltonians as

$$\begin{aligned} H_{ex} = -m_0 \cdot J_z e^{-r/r_0} = -m_0 \left(L_z + \frac{\sigma_z}{2}\right) e^{-r/r_0} \\ H_{SOC} = -\lambda_0 \cdot L_z \sigma_z e^{-r/r_0} \end{aligned} \tag{25}$$

where m_0 and λ_0 are parameters controlling the strength of the exchange coupling and spin-orbit coupling respectively.

2.6 Helical band

In the bulk of most materials, the electrons have an energy relation similar to that in real space, with their kinetic energy being proportional to the square of their momentum. However, his relation doesn't nescessarily hold on the surface of materials. At the interface of a superconductor and a topological insulator, electrons behave differently due to the metallic states at the surface of such an insulator. However, it is also believed that such a topological surface state can occur on the surface of materials like Fe(Te,Se)[12], which is the impertus of [3] to investigate this helical band. In such a topological surface state, the non-interacting part

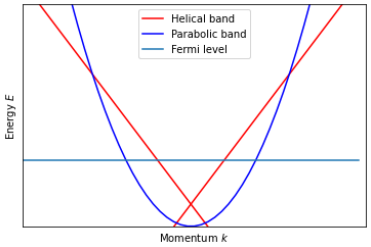

Figure 1: Dispersion relation for a helical and parabolic band, based on [3].

of the Hamiltonian is given by the Rashba Hamiltonian:

$$\int \mathrm{d}\boldsymbol{r}\psi^\dagger(\boldsymbol{r})[v_D(\boldsymbol{\sigma}\times\boldsymbol{\pi})\cdot\hat{z}-\varepsilon_F]\psi(\boldsymbol{r}) \tag{26}$$

Where $\boldsymbol{\pi}$ is the canonical momentum and v_D is the Dirac velocity of the electrons in this particular material. This Rashba Hamiltonian means that the helical band is radically different than the bulk parabolic band, and as such potentially has different properties than the bulk band. The different properties can in part be seen by comparing the dispersion relation for the parabolic and the helical band, as done on figure 1. For our purposes, the most interesting property of this helical band is the fact that an extra phase is acquired by the $u(\boldsymbol{r})$ and $v(\boldsymbol{r})$ wavefuntions. This means that for the case of a vortex, there are modes with no angular momentum, and one of these modes is a Majorana zero mode[7][3]. The Majorana zero mode is characterized by being it's own antiparticle: $\gamma_0^\dagger=\gamma_0$. We can write this operator as[8]:

$$\gamma_0^\dagger=\int d^2\boldsymbol{r}[u_{0\uparrow}(r)\psi_\uparrow^\dagger(\boldsymbol{r})+v_{0\uparrow}(r)\psi_\uparrow(\boldsymbol{r})+u_{0\downarrow}(r)e^{i\theta}\psi_\downarrow^\dagger(\boldsymbol{r})+v_0(r)e^{-i\theta}\psi_\downarrow(\boldsymbol{r})] \tag{27}$$

Using this equation, we see that the MZM needs to follow the relations $u_{0\uparrow}(r)=v_{0\uparrow}(r)$ and $u_{0\downarrow}(r)=v_{0\downarrow}(r)$. This allows us to check whether any zero-energy mode we get is in fact a MZM.

3 Bessel decomposition of the BdG equations

Now that we know the BdG equations, the next step is to solve them. Since we want to consider complicated setups where we have both a vortex and a magnetic impurity, we need to look at numerical solutions. We will be using a method similar to the one used in [3], and write all of our functions in terms of Bessel functions. To do this, we consider a disc of radius R, such that we have the cylindrical symmetry that makes Bessel functions a reasonable choice[5]. We start out by considering an ordinary parabolic band. For simplicity, we can supress the spin dependency of $u_{n\sigma}$ and $v_{n\sigma}$, since our basic Hamiltonian is spin-symmetric.
We want to analyze the case where ν flux quanta are passing through the middle of our disc, where $\nu=\{0,1\}$. This flux is introduced by writing our gap as $\Delta(\boldsymbol{r})=\Delta(r)e^{i\nu\theta}$. This means that $\Delta(\boldsymbol{r})$ isn't necessarily real everywhere. To make it real, we can perform a gauge transformation $\Delta(\boldsymbol{r})\to\Delta(\boldsymbol{r})e^{-2ie\chi(\boldsymbol{r})}$, as long as we also perform comparable transformations $\boldsymbol{A}\to\boldsymbol{A}+\nabla\chi(\boldsymbol{r})$, and $u_n(\boldsymbol{r})\to u_n(\boldsymbol{r})e^{-ie\chi(\boldsymbol{r})}$, $v_n(\boldsymbol{r})\to v_n(\boldsymbol{r})e^{ie\chi(\boldsymbol{r})}$. We can see from equation (23) that the phase of $\Delta(\boldsymbol{r})$ is equal to the phase of $u_n(\boldsymbol{r})v_n^*(\boldsymbol{r})$. As such, we can write these functions as:

$$u_n(\boldsymbol{r})=u_n(r)e^{i\phi(\boldsymbol{r})}e^{i\frac{\nu}{2}\theta}\quad v_n(\boldsymbol{r})=v_n(r)e^{i\phi(\boldsymbol{r})}e^{-i\frac{\nu}{2}\theta} \tag{28}$$

Now, we demand that u_n and v_n are invariant under a 2π rotation, so $\phi(\boldsymbol{r})=\mu\theta$ where $\mu\pm\frac{\nu}{2}\in\mathbb{Z}$. Now, we can consider the case of $\nu=0$ and $\nu=1$ separately.

3.1 Without vortex

For the case without a vortex, $\nu = 0$ and a such $\Delta(\boldsymbol{r}) = \Delta(r)$ which is real everywhere. As such, we see that

$$[u_{nl}(\boldsymbol{r}), v_{nl}(\boldsymbol{r})] = [u_{nl}(r), v_{nl}(r)]e^{il\theta} \tag{29}$$

Where $l \in \mathbb{Z}$. We plug this into (22)

$$\begin{pmatrix} -\frac{1}{2m}(\nabla + ie\boldsymbol{A})^2 & \Delta(r) \\ \Delta(r) & \frac{1}{2m}(\nabla - ie\boldsymbol{A})^2 \end{pmatrix} e^{il\theta} \begin{pmatrix} u_{nl}(r) \\ v_{nl}(r) \end{pmatrix} = E_{nl} e^{il\theta} \begin{pmatrix} u_{nl}(r) \\ v_{nl}(r) \end{pmatrix} \tag{30}$$

Multiplying the exponential factor into the matrix and multiplying both sides by $e^{-il\theta}$, we get

$$\begin{pmatrix} -\frac{1}{2m}(\nabla + i\frac{l}{r}\hat{\theta} + ie\boldsymbol{A})^2 & \Delta(r) \\ \Delta(r) & \frac{1}{2m}(\nabla + i\frac{l}{r}\hat{\theta} - ie\boldsymbol{A})^2 \end{pmatrix} \begin{pmatrix} u_{nl}(r) \\ v_{nl}(r) \end{pmatrix} = E_{nl} \begin{pmatrix} u_{nl}(r) \\ v_{nl}(r) \end{pmatrix} \tag{31}$$

Now, we consider the size of $\boldsymbol{A}$. Since we care about a type-II superconductor, $\xi \ll \lambda$. This equivalently means that $\boldsymbol{A} \ll \frac{l}{er}$[3]. Therefore, we can ignore $\boldsymbol{A}$, and the equation we want to solve is

$$\begin{pmatrix} -\frac{1}{2m}(\nabla + i\frac{l}{r}\hat{\theta})^2 & \Delta(r) \\ \Delta(r) & \frac{1}{2m}(\nabla + i\frac{l}{r}\hat{\theta})^2 \end{pmatrix} \begin{pmatrix} u_{nl}(r) \\ v_{nl}(r) \end{pmatrix} = E_{nl} \begin{pmatrix} u_{nl}(r) \\ v_{nl}(r) \end{pmatrix} \tag{32}$$

We now expand the diagonal terms, throwing away the θ-dependent terms since $u_{nl}(r)$ and $v_{nl}(r)$ only depend on r:

$$(\nabla + i\frac{l}{r}\hat{\theta})^2 = \partial_r^2 + \frac{1}{r}\partial_r - \left(\frac{l}{r}\right)^2 \tag{33}$$

The right hand side looks a lot like Bessel's equation, which has the form

$$r^2\partial_r^2 f + r\partial_r f + (r^2 - \mu^2)f = 0 \tag{34}$$

This is solved by Bessel functions $J_\mu(r)$, and as such, we want to write $u_{nl}(r)$ and $v_{nl}(r)$ in terms of this function. Bessel functions obey an orthogonality relation

$$\frac{1}{R^2}\int_0^R \mathrm{d}r r J_\mu\left(\frac{\beta_{i\mu}\cdot r}{R}\right) J_\mu\left(\frac{\beta_{j\mu}\cdot r}{R}\right) = \frac{\delta_{ij}}{2} J_{\mu+1}(\beta_{i\mu})$$

where $\beta_{i\mu}$ is the i'th zero of the μ'th Bessel function. We thus define:

$$[u_{nl}(r), v_{nl}(r)] = \sum_{j=1}^{J} [u_{nlj}, v_{nlj}]\phi_{lj}(r) \tag{35}$$

Where

$$\phi_{lj} = \frac{\sqrt{2}}{RJ_{l+1}(\beta_{jl})} J_l\left(\frac{\beta_{jl}\cdot r}{R}\right) \tag{36}$$

Strictly speaking, we want $J = \infty$ for this equality to hold, but since this equation is going to be solved numerically we impose a cutoff. Plugging this into the top line of (32), we get

$$\begin{aligned} \sum_{j=1}^{J} -\frac{1}{2m}\left(\partial_r^2 + \frac{1}{r}\partial_r - \left(\frac{l}{r}\right)^2\right)\phi_{lj}(r)u_{nlj} + \sum_{j=1}^{J}\Delta(r)v_{nlj}\phi_{lj}(r) \\ = E_{nl}\sum_{j=1}^{J} u_{nlj}\phi_{lj}(r) \end{aligned} \tag{37}$$

Now, we can use the fact that J_μ obeys Bessel's equation to write

$$\sum_{j=1}^{J} \frac{1}{2m} \left(\frac{\beta_{jl}}{R}\right)^2 \phi_{lj}(r) u_{nlj} + \sum_{j=1}^{J} \Delta(r) v_{nlj} \phi_{lj}(r) = E_{nl} \sum_{j=1}^{J} u_{nlj} \phi_{lj}(r) \tag{38}$$

We can now multiply this equation on both sides by $r \cdot \phi_{lj'}$ and integrate over r to get

$$\frac{1}{2m} \left(\frac{\beta_{jl}}{R}\right)^2 u_{nlj} + \sum_{j'=1}^{J} \int_0^R \mathrm{d}r \Delta(r) r v_{nlj} \phi_{lj'} \phi_{lj} = E_{nl} u_{nlj} \tag{39}$$

If we do the same calculation for the lower line of (32), we get

$$\begin{pmatrix} T & \Delta \\ \Delta & -T \end{pmatrix} \begin{pmatrix} \overline{u_{nl}} \\ \overline{v_{nl}} \end{pmatrix} = E_{nl} \begin{pmatrix} \overline{u_{nl}} \\ \overline{v_{nl}} \end{pmatrix} \tag{40}$$

Where $T_{ij} = \frac{\beta_{jl}^2}{R^2} \delta_{ij}$ and $\Delta_{ij} = \sum_{j=1}^{J} \int_0^R \mathrm{d}r \Delta(r) r \phi_{li} \phi_{lj}$. We also define $\overline{u_{nl}} = (u_{nl1}, u_{nl2}...)^T$ and $\overline{v_{nl}} = (v_{nl1}, v_{nl2}...)^T$

3.2 Vortex

For the case with a vortex where $\nu = 1$, a lot of the methods are the same as above, but with a few changes. If we start out by performing a gauge transformation so that Δ is real, we can use $\chi = \frac{1}{2}\theta$, and we get $\boldsymbol{A} \to \boldsymbol{A} + \frac{1}{2er}\hat{\theta}$. We can also use the fact that $\mu + \frac{\nu}{2}$ must be an integer to see that μ must be a half-integer. With this information, we can begin solving (22)

$$\begin{pmatrix} -\frac{1}{2m}(\nabla + ie(\boldsymbol{A} + \frac{1}{2er}\hat{\theta}))^2 & \Delta(r) \\ \Delta(r) & \frac{1}{2m}(\nabla - ie(\boldsymbol{A} + \frac{1}{2er}\hat{\theta}))^2 \end{pmatrix} e^{i\mu\theta} \begin{pmatrix} u_{n\mu}(r) \\ v_{n\mu}(r) \end{pmatrix} = E_{n\mu} e^{i\mu\theta} \begin{pmatrix} u_{n\mu}(r) \\ v_{n\mu}(r) \end{pmatrix} \tag{41}$$

We can throw away $\boldsymbol{A}$ and multiply $e^{i\mu\theta}$ into the matrix following the same procedure as above, which gives us

$$\begin{pmatrix} -\frac{1}{2m}(\nabla + i(\frac{\mu+\frac{1}{2}}{r}\hat{\theta}))^2 & \Delta(r) \\ \Delta(r) & \frac{1}{2m}(\nabla - i(\frac{\mu-\frac{1}{2}}{r}\hat{\theta}))^2 \end{pmatrix} \begin{pmatrix} u_{n\mu}(r) \\ v_{n\mu}(r) \end{pmatrix} = E_{n\mu} \begin{pmatrix} u_{n\mu}(r) \\ v_{n\mu}(r) \end{pmatrix} \tag{42}$$

We will now define $\mu^+ = \mu + \frac{1}{2}$ and $\mu^- = \mu - \frac{1}{2}$ for convenience. Now, we once again recognize that the diagonal terms are similar to Bessel's equation, but this time of order $\mu \pm \frac{1}{2}$. Since the two Bessel equations are different, we decompose u and v in different ways

$$\begin{aligned} u_{n\mu^+} &= \sum_{j=1}^{J} u_{n\mu^+ j} \phi_{\mu^+ j}(r) \\ v_{n\mu^-} &= \sum_{j=1}^{J} v_{n\mu^- j} \phi_{\mu^- j}(r) \end{aligned} \tag{43}$$

Plugging this into the top line of (42) and using the properties of Bessel functions, we get

$$\sum_{j=1}^{J} \frac{1}{2m} \left(\frac{\beta_{j\mu^+}}{R}\right)^2 \phi_{\mu^+ j}(r) u_{n\mu^+ j} + \sum_{j=1}^{J} \Delta(r) v_{n\mu^- j} \phi_{\mu^- j}(r) = E_{n\mu} \sum_{j=1}^{J} u_{n\mu^+ j} \phi_{\mu^+ j}(r) \tag{44}$$

We can multiply this through by $r\phi_{\mu^+ j'}$ and integrate with respect to r to obtain a final equation:

$$\frac{1}{2m} \left(\frac{\beta_{j\mu^+}}{R}\right)^2 u_{n\mu^+ j} + \sum_{j'=1}^{J} \int_0^R \mathrm{d}r \Delta(r) v_{n\mu^- j'} \phi_{\mu^- j'} \phi_{\mu^+ j}(r) r = E_{n\mu} u_{n\mu^+ j} \tag{45}$$

Doing the same calculation for the lower line of (42), we get the matrix equation

$$\begin{pmatrix} T_{\mu^+} & \Delta_{\mu^+\mu^-} \\ \Delta^T_{\mu^+\mu^-} & -T_{\mu^-} \end{pmatrix} \begin{pmatrix} \overline{u}_{n\mu^+} \\ \overline{v}_{n\mu^-} \end{pmatrix} = E_{n\mu} \begin{pmatrix} \overline{u}_{n\mu^+} \\ \overline{v}_{n\mu^-} \end{pmatrix} \tag{46}$$

Where $T^{\mu^\pm}_{ij} = \frac{1}{2m}\left(\frac{\beta_{j\mu^\pm}}{R}\right)^2 \delta_{ij}$ and

$$\Delta^{\mu^+\mu^-}_{ij} = \int_0^r \mathrm{d}r \Delta(r)\phi_{\mu^+ i}(r)\phi_{\mu^- j}(r)r \tag{47}$$

3.3 Helical band

We also want to find the Bessel decomposition of the helical band, which is given by the Hamiltonian $H'_{kin} = v_D(\boldsymbol{\sigma} \times \boldsymbol{\pi}) \cdot \hat{z} + \varepsilon_F$. Ignoring the Fermi energy, this can be rewritten:

$$v_D(\boldsymbol{\sigma} \times \boldsymbol{\pi}) \cdot \hat{z} = v_D(\sigma_x \pi_y - \sigma_y \pi_x) \tag{48}$$

This time, the Hamiltonian depends on the spin, so we need the full Nambu spinor. We start by considering the case where $\nu = 0$. In this case, $\Delta(\boldsymbol{r}) = \Delta(r)$, and we don't need to transform $\boldsymbol{A}$. Thus, we can simply let $\pi_i = p_i$, so we get

$$v_D(\sigma_x p_y - \sigma_y p_x) = -i\hbar v_D(\sigma_x \partial_y - \sigma_y \partial_x) = -i\hbar v_D \sigma_y e^{-i\sigma_z\theta}(\partial_r - i\sigma_z \frac{\partial_\theta}{r}) \tag{49}$$

Now, we want to solve the Schrödinger equation for this Hamiltonian. We use the fact [7] that the Hamiltonian commutes with the angular momentum operator to find simultaneous eigenstates of the two operators. We start by considering $J|\mu\rangle = \mu|\mu\rangle$, looking only at u_σ for simplicity

$$J|\mu\rangle = \left(-i\partial_\theta + \frac{\sigma_z}{r}\right)\begin{pmatrix} u_\uparrow \\ u_\downarrow \end{pmatrix} \tag{50}$$

We now use the ansatz that

$$\begin{pmatrix} u_\uparrow \\ u_\downarrow \end{pmatrix} = \begin{pmatrix} u_\uparrow(r)e^{i(\mu - \frac{1}{2}\theta)} \\ u_\downarrow(r)e^{i(\mu+\frac{1}{2}\theta)} \end{pmatrix} \tag{51}$$

Where μ is a half-integer to make sure that our function is single-valued. Plugging this in, we get:

$$J\begin{pmatrix} u_\uparrow(r)e^{i(\mu - \frac{1}{2}\theta)} \\ u_\downarrow(r)e^{i(\mu+\frac{1}{2}\theta)} \end{pmatrix} = \mu\begin{pmatrix} u_\uparrow(r)e^{i(\mu - \frac{1}{2}\theta)} \\ u_\downarrow(r)e^{i(\mu+\frac{1}{2}\theta)} \end{pmatrix} \tag{52}$$

So our ansatz does constitute an angular momentum eigenstate. We can now plug our ansatz into the Schrödinger equation:

$$\hbar v_D \begin{pmatrix} 0 & e^{-i\theta}(\partial_r - i\frac{\partial_\theta}{r}) \\ -e^{i\theta}(\partial_r + i\frac{\partial_\theta}{r}) & 0 \end{pmatrix}\begin{pmatrix} u_\uparrow(r)e^{i(\mu - \frac{1}{2}\theta)} \\ u_\downarrow(r)e^{i(\mu+\frac{1}{2}\theta)} \end{pmatrix} = E_\mu \begin{pmatrix} u_\uparrow(r)e^{i(\mu - \frac{1}{2}\theta)} \\ u_\downarrow(r)e^{i(\mu+\frac{1}{2}\theta)} \end{pmatrix} \tag{53}$$

Considering only the top equation, we get:

$$\hbar v_D e^{-i\theta}(\partial_r - i\frac{\partial_\theta}{r})u_\downarrow(r)e^{i\mu^+\theta} = E u_\uparrow(r)e^{i\mu^-\theta} \to \hbar v_D(\partial_r + \frac{\mu^+}{r})u_\downarrow(r) = E_\mu u_\uparrow(r) \tag{54}$$

Where $\mu^+ = \mu + \frac{1}{2}$ and $\mu^- = \mu - \frac{1}{2}$.Doing the same for the bottom equation, we can write the Hamiltonian:

$$\hbar v_D \begin{pmatrix} 0 & (\partial_r + \frac{\mu^+}{r}) \\ -(\partial_r - \frac{\mu^-}{r}) & 0 \end{pmatrix}\begin{pmatrix} u_\uparrow(r) \\ u_\downarrow(r) \end{pmatrix} = E_\mu \begin{pmatrix} u_\uparrow(r) \\ u_\downarrow(r) \end{pmatrix} \tag{55}$$

As such, while we are indexing with half-integers, we still only get integer Bessel functions, and indeed could shift everything by a constant phase to index with integers instead, letting $\mu^- = l$ and $\mu^+ = l + 1$.
We now do the same thing for v_σ. The corresponding ansatz is very similar:

$$\begin{pmatrix} v_\downarrow \\ -v_\uparrow \end{pmatrix} = \begin{pmatrix} v_\downarrow(r)e^{i(\mu - \frac{1}{2}\theta)} \\ -v_\uparrow(r)e^{i(\mu+\frac{1}{2}\theta)} \end{pmatrix} \tag{56}$$

The Hamiltonian, however, is slightly different[8]:

$$H_v = -\sigma_y H_u^* \sigma_y = \hbar v_D \begin{pmatrix} 0 & -e^{-i\theta}(\partial_r - i\frac{\partial_\theta}{r}) \\ e^{i\theta}(\partial_r + i\frac{\partial_\theta}{r}) & 0 \end{pmatrix} \tag{57}$$

Solving the Schrodinger equation for this Hamiltonian with the ansatz above gives the following equation:

$$\hbar v_D \begin{pmatrix} 0 & -(\partial_r + \frac{\mu^+}{r}) \\ (\partial_r - \frac{\mu^-}{r}) & 0 \end{pmatrix} \begin{pmatrix} v_\downarrow(r) \\ -v_\uparrow(r) \end{pmatrix} = E_\mu \begin{pmatrix} v_\downarrow(r) \\ -v_\uparrow(r) \end{pmatrix} \tag{58}$$

Putting the Fermi energy back in, the complete BdG equations then become:

$$\begin{pmatrix} \varepsilon_F & \hbar v_D(\partial_r + \frac{\mu^+}{r}) & \Delta(r) & 0 \\ -\hbar v_D(\partial_r - \frac{\mu^-}{r}) & \varepsilon_F & 0 & \Delta(r) \\ \Delta(r) & 0 & -\varepsilon_F & -\hbar v_D(\partial_r + \frac{\mu^+}{r}) \\ 0 & \Delta(r) & \hbar v_D(\partial_r - \frac{\mu^-}{r}) & -\varepsilon_F \end{pmatrix} \begin{pmatrix} u_\uparrow(r) \\ u_\downarrow(r) \\ v_\downarrow(r) \\ -v_\uparrow(r) \end{pmatrix} = E_\mu \begin{pmatrix} u_\uparrow(r) \\ u_\downarrow(r) \\ v_\downarrow(r) \\ -v_\uparrow(r) \end{pmatrix} \tag{59}$$

We now follow a procedure very similar to the one in the case of a parabolic band. We write the u_σ and v_σ functions in terms of normalized Bessel functions:

$$\begin{aligned} u_{nl\sigma}(r) &= \sum_i u_{nli\sigma}\phi_{li}(r) \\ v_{nl\sigma}(r) &= \sum_i v_{nli\sigma}\phi_{li}(r) \end{aligned} \tag{60}$$

Where $\phi_{li}(r)$ is defined in (36). If we consider the top line of the BdG equation, we get:

$$\varepsilon_F \sum u_{n\mu^- i\uparrow}\phi_{\mu^- i}(r) + \hbar v_D(\partial_r + \frac{\mu^+}{r}) \sum u_{n\mu^+ i\downarrow}\phi_{\mu^+ i}(r) + \Delta(r) \sum v_{n\mu^- i\uparrow}\phi_{\mu^- i}(r) = E_l \sum u_{n\mu^- i\uparrow}\phi_{\mu^- i}(r) \tag{61}$$

We then multiply both sides by $r \cdot \phi_{\mu^- j}$ and take the integral from 0 to R. Doing this yields the equation:

$$\varepsilon_F \sum u_{n\mu^- i\uparrow} + V_{\mu^-,\mu^+} u_{n\mu^+ i\downarrow} + \sum_j \int_0^R \mathrm{d}r \Delta(r) v_{n\mu^- i\uparrow}\phi_{\mu^- i}(r)\phi_{\mu^- j} = E_l u_{n\mu^- i\uparrow} \tag{62}$$

Where

$$V_{i,j}^{\mu^-,\mu^+} = \frac{\beta_{i\mu^-} \cdot \beta_{j\mu^+}}{\beta_{i\mu^-}^2 - \beta_{j\mu^+}^2} \tag{63}$$

As shown in appendix A. Doing the same thing for the other lines of the equation, we finally get the equation:

$$\begin{pmatrix} \varepsilon_F & V_{\mu^-,\mu^+} & \Delta_{\mu^-} & 0 \\ V_{\mu^-,l^+}^T & \varepsilon_F & 0 & \Delta_{\mu^+} \\ \Delta_{\mu^-}^T & 0 & -\varepsilon_F & -V_{\mu^-,\mu^+} \\ 0 & \Delta_{\mu^+}^T & -V_{\mu^-,\mu^+}^T & -\varepsilon_F \end{pmatrix} \begin{pmatrix} \overline{u_{n\mu^-\uparrow}} \\ \overline{u_{n\mu^+\downarrow}} \\ \overline{v_{n\mu^-\downarrow}} \\ -\overline{v_{n\mu^+\uparrow}} \end{pmatrix} = E_\mu \begin{pmatrix} \overline{u_{n\mu^-\uparrow}} \\ \overline{u_{n\mu^+\downarrow}} \\ \overline{v_{n\mu^-\downarrow}} \\ -\overline{v_{n\mu^+\uparrow}} \end{pmatrix} \tag{64}$$

Where $\Delta_{ij}^{\mu^\pm} = \int_0^R \mathrm{d}r \Delta(r)\phi_{\mu^\pm i}(r)\phi_{\mu^\pm j}(r)$.

3.3.1 Vortex

In the case where we have a vortex, we use a slightly different approach. This time, we need to carry $\boldsymbol{A}$ along, so we end up with a Hamiltonian of the form:

$$-i\hbar v_D \sigma_y e^{-i\sigma_z\theta}(\partial_r - i\sigma_z\frac{\partial_\theta}{r}) + v_D e\sigma_x A_y - v_D e\sigma_y A_x \tag{65}$$

Since $\Delta(\boldsymbol{r}) = e^{i\nu\theta}\Delta(r)$, we need to perform a gauge transformation to make Δ real everywhere. This transformation $\Delta(\boldsymbol{r}) \to \Delta(r)$ also transforms $\boldsymbol{A} \to \boldsymbol{A} + \frac{1}{2er}\hat{\theta}$. If we now assume $\boldsymbol{A}$ is negligible as above, we get:

$$-i\hbar v_D \sigma_y e^{-i\sigma_z\theta}(\partial_r - i\sigma_z\frac{\partial_\theta}{r}) + v_D\sigma_x\frac{\sin\theta}{2r} - v_D\sigma_y\frac{\cos\theta}{2r} \tag{66}$$

Which can be rewritten as:

$$-i\hbar v_D \sigma_y e^{-i\sigma_z\theta}(\partial_r - i\left(\sigma_z\frac{\partial_\theta}{r} - \sigma_z\frac{1}{2r}\right)) \tag{67}$$

Since we've performed a gauge transformation, we no longer necessarily want the wavefunctions to return to themselves under a 2π rotation. However, we can use the structure of the Hamiltonian to make an ansatz

$$\begin{pmatrix} u_\uparrow \\ u_\downarrow \\ v_\downarrow \\ -v_\uparrow \end{pmatrix} = \begin{pmatrix} u_\uparrow(r)e^l \\ u_\downarrow(r)e^{l+1} \\ v_\downarrow(r)e^{l-1} \\ -v_\uparrow(r)e^l \end{pmatrix} \tag{68}$$

Plugging this into the Hamiltonian along with the Fermi energy, we get the following structure:

$$\begin{pmatrix} \varepsilon_F & \hbar v_D(\partial_r + \frac{l+1}{r}) & \Delta(r) & 0 \\ -\hbar v_D(\partial_r - \frac{l}{r}) & \varepsilon_F & 0 & \Delta(r) \\ \Delta(r) & 0 & -\varepsilon_F & -\hbar v_D(\partial_r + \frac{l}{r}) \\ 0 & \Delta(r) & \hbar v_D(\partial_r - \frac{l-1}{r}) & -\varepsilon_F \end{pmatrix} \begin{pmatrix} u_\uparrow(r) \\ u_\downarrow(r) \\ v_\downarrow(r) \\ -v_\uparrow(r) \end{pmatrix} = E_l \begin{pmatrix} u_\uparrow(r) \\ u_\downarrow(r) \\ v_\downarrow(r) \\ -v_\uparrow(r) \end{pmatrix} \tag{69}$$

Which implies that l is an integer. This also makes sense intuitively, as adding a vortex is equivalent to shifting the phase of u_σ and v_σ by one half in different directions.

We now do the Bessel decomposition on a very similar way. Since $u_\uparrow, v_\uparrow$ and $u_\downarrow, v_\downarrow$ no longer have the same angular momenta, we get a different form of the Δ term:

$$\Delta_{i,j}^{l,l'} = \int \mathrm{d}r\Delta(r)r\phi_{li}(r)\phi_{l'j}(r) \tag{70}$$

We end up getting the equation:

$$\begin{pmatrix} \varepsilon_F & V_{l,l+1} & \Delta_{l,l-1} & 0 \\ V_{l,l+1}^T & \varepsilon_F & 0 & \Delta_{l+1,l} \\ \Delta_{l,l-1}^T & 0 & -\varepsilon_F & -V_{l-1,l} \\ 0 & \Delta_{l+1,l}^T & -V_{l-1,l}^T & -\varepsilon_F \end{pmatrix} \begin{pmatrix} \overline{u_{n,l\uparrow}} \\ \overline{u_{n,l+1\downarrow}} \\ \overline{v_{n,l-1\downarrow}} \\ -\overline{v_{n,l\uparrow}} \end{pmatrix} = E_\mu \begin{pmatrix} \overline{u_{n,l\uparrow}} \\ \overline{u_{n,l+1\downarrow}} \\ \overline{v_{n,l-1\downarrow}} \\ -\overline{v_{n,l\uparrow}} \end{pmatrix} \tag{71}$$

We can also use our decomposition into angular momentum states to analyze the MZM that might be present in a helical band superconductor. To do this, we consider equation (69) in the case where $l = 0$. In addition, we look for a solution where $E = 0$. In

3.4 Extra terms

When doing the calculations, we also want to include the terms generated by the exchange and spin-orbit interactions given by the Hamiltonians in (25).

We can write $L_z = -i\hbar\partial_\theta$. Applying this to our functions $u_{nl\sigma}$ and $v_{nl\sigma}$, we see that in this basis we can write $L_z = \tau_z l$, where l is the angular momentum quantum number and τ_z is the electron-hole Pauli matrix. As such, we can write the ion-induced terms as:

$$H_{ion} = -(m_0 l\tau_z e^{-r/r_0} + \frac{m_0}{2}\sigma_z e^{-r/r_0} - \lambda_0 l\tau_z\sigma_z e^{-r/r_0}) \tag{72}$$

This is then added to the kinetic Hamiltonian and put into the BdG equations. Once the Bessel decomposition is done, we get the following matrix, in the case of $\nu = 0$:

$$H_{ion} = \begin{pmatrix} -(L+M+\Lambda)_l & 0 & 0 & 0 \\ 0 & -(L-M-\Lambda)_l & 0 & 0 \\ 0 & 0 & -(L+M-\Lambda)_l & 0 \\ 0 & 0 & 0 & -(L-M+\Lambda)_l \end{pmatrix} \tag{73}$$

Where

$$[L_{ij}, M_{ij}, \Lambda_{ij}]_l = [lm_0, \frac{m_0}{2}, \lambda_0 l]\int_0^R \mathrm{d}r\ r\phi_{li}(r)e^{-r/r_0}\phi_{lj}(r) \tag{74}$$

The angular momenta used varies from case to case, but the general form of the expressions is always the same. This allows for computational efficiency, since the integrals can be computed once ahead of time and then used repeatedly. The full matrices that we're using are provided in appendix B.

3.5 Numerical analysis

We now have an equation for finding $u(r)$ and $v(r)$ given $\Delta(r)$, as well as an equation for finding $\Delta(r)$ given $u(r)$ and $v(r)$. As such, we can find $\Delta(r)$ self-consistenly: We start out with a qualified guess of the form of Δ, and then we repeatedly find Δ, u and v until our Δ converges. This is done computationally.

To solve these equations computationally, we need to write them in a dimensionless form. We use the same non-dimensionalization as in [8]. we define l_0 such that $\frac{\hbar^2}{2m^* l_0^2} = 10\text{meV}$. We use this as our length scale, and 10 meV as our energy scale E_0. For specific numerical values, we used the ones provided in [3] for iron tellurium selenium, so we used $\varepsilon_F = 4.52$ meV, $g = 11$ meV, $\omega_D = 4.7$ meV. These values gives $\xi = 2.8l_0$. We also chose $r_0 = 2l_0$. These parameters are designed to give a bulk gap of $\Delta_0 = 1.5$ meV. For the helical band, we used similar parameters, but this time needed to include a Dirac velocity v_D. For this, we used 7.5 eV$\cdot l_0$, which gave a gap value of around 1.0 eV. We chose this v_D rather than the value provided in [3] to get a gap that was more comparable with that of the bulk case.

To actually compute the matrix elements in (46), we need to perform a bunch of integrals. To perform these efficiently, we discretize the inteval from 0 to R into 750 points and do a sum over these points. In addition, we compute the values of ϕ_{lj} at each of these 750 points for all relevant values of l and j[10]. We use j ranging from 0 to 199 for all calculations, but the range of l depends on the exact computation, since different computations require different compromises between speed and accuracy. For all of the plots apart from the energy calculation, we used a range of 200 angular momenta, while we used only 150 angular momenta for the energy calculation to save time since the result didn't qualitatively change if we used higher numbers. These numbers include both the positive and negative momenta.

For the graphs of Δ, we iterated this code until the value of Δ at $\xi/2$ changed by less than 1% between

iterations. For the energy graphs, it was important that all cases had the same amount of iterations, so we chose to do three iterations in all cases. We chose this since that was usually the number of iterations that it did when we used the other criteria, and it only changed by a few percent if we did more iterations.

4 Results

We started out by considering the simplest possible case: No spin-orbit or exchange interaction, and no vortex. In this case, we expect to get a constant Δ and no sub-gap states. However, this is not exactly what we get. Due to the fact that we only use a finite amount of angular momenta in our computations, we get a decay near the edge of the disc, as can be seen on figure 2.

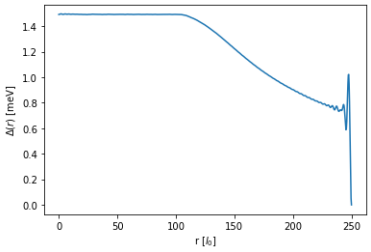

Figure 2: Δ calculated without any vortex or impurity present.

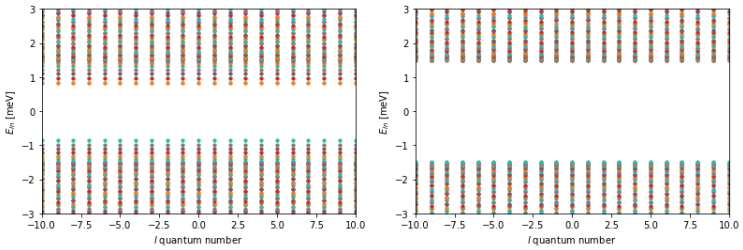

Figure 3: Right: Energy spectrum for $\nu = 0$ without fixed edge values. Left: Energy spectrum for $\nu = 0$ with fixed edge values.

This isn't actually too surprising[8], and simply means that we have to be careful when we look at the edge of the disc. We also get some in-gap states, which occur due to this "fuzzy" edge. If we simply set the edge to always be constant, these states disappear, as can be seen on figure 3.

We then considered the case of a vortex being present without any impurities. Near the vortex, Δ is supressed, as can be seen in figure 4. The oscillations of Δ are expected [3], and as such this calculation is a good indication that our program is working as expected.

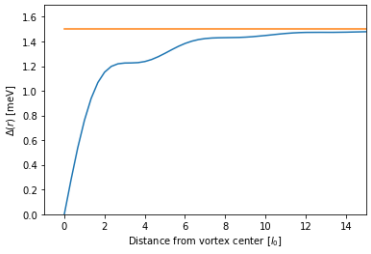

Figure 4: The blue curve is $\Delta(r)$ at a vortex. The orange curve is the value away from a vortex.

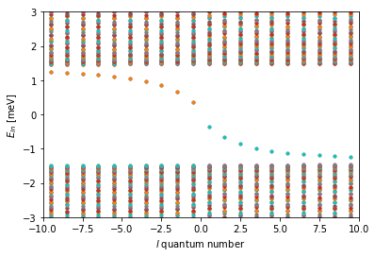

Figure 5: Energy spectrum for a superconductor with a vortex.

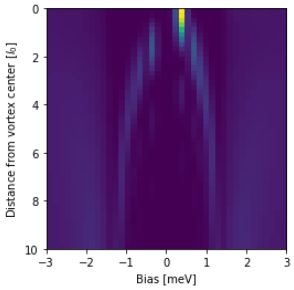

Figure 6: Density of states near a vortex.

We saw CdGM states inside the superconducting gap, as can be seen on figure 5. From analytical results, we expect these to follow the relation $E = \mu\frac{\Delta^2}{\varepsilon_F}$. We see that this holds roughly for small μ, but breaks

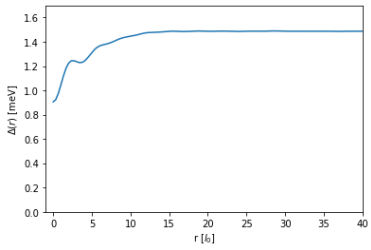

Figure 7: $\Delta(r)$ near a magnetic impurity.

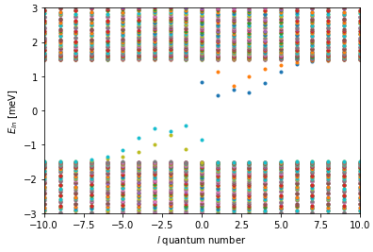

Figure 8: Energy spectrum of magnetic impurity.

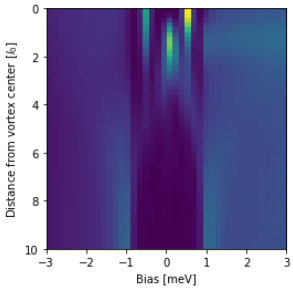

Figure 9: DOS near a magnetic impurity.

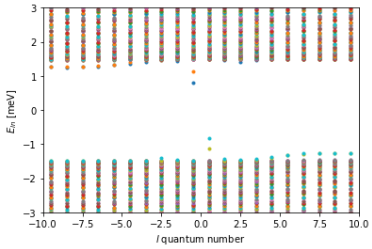

Figure 10: Energy spectrum of a vortex at a magnetic impurity.

down fairly quickly. This is unsurprising, since the relation is in the limit where $\Delta \ll \varepsilon_F$, which is not the limit we're working in. We also calculated the local density of states, shown on figure 6, and saw that the CdGM states are clearly visible. We notice that the density of states is asymmetric. This is explained by the fact that in our Hamiltonian, the electron with angular momentum l corresponds to the hole with angular momentum $l + 1$.

We now turn on the exchange and spin-orbit coupling. This has a different effect depending on whether we look at the case with or without a vortex. For the case without a vortex, this slightly suppresses Δ around the magnetic impurity, which can bee seen on figure 7. This suppression allows for sub-gap states, which can be seen on both the energy spectrum on figure 8 and on the density of states plot. We can also use the density of states plot to see that these states are spin-polarized, since the exchange and spin-orbit coupling means that spin-symmetry is broken in the system.

In the case of a vortex, $\Delta(r)$ actually goes to the bulk value faster than without an impurity, and the CdGM states are pushed outwards, as can be seen on figure 10. The fact that the CdGM states are pushed outwards turns out to be significant, since it means a magnetic impurity lowers the energy of the vortex. This means that, for some impurity strength m_0, the vortex potentially has a lower energy than the non-vortex case, and as such a vortex can spontaneously form around an impurity. To analyze this, we ran our program for a range of m_0 for both the vortex and vortex-free case. This allowed us to calculate the vortex binding energy $E_{vb} = E_{vortex} - E_{vortex-free}$, which is the energy of a single vortex.

The energy of any given state has a number of terms. The most important term is the term from all of the occupied states. When calculating this term, it is important to be cognizant of the fact that the vortex free case has integer-indexed states, while the vortex case has half-integer indexed states. This means that the number of states between $-L$ and L is an odd number for the vortex-free case, but an even number for the

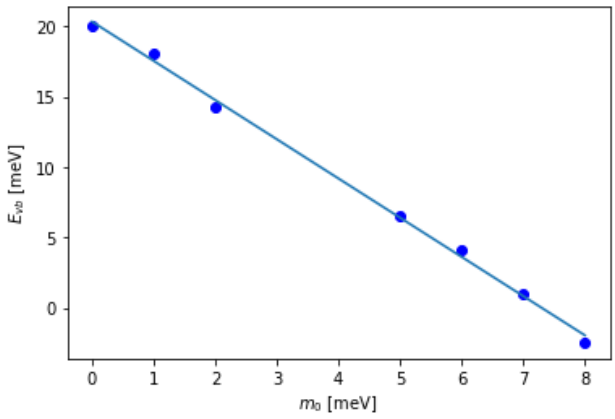

Figure 11: E_{vb} for various m_0, with a line of best fit.

vortex case. When computing the energy difference between two cases, it's important that we sum over the same amount of angular momenta for each state. This runs into an issue, as the even number of angular momenta in one case doesn't match the odd number of angular momenta in another case. The solution is to throw away one angular momenta. Through simple testing, it turns out that cutting either the maximum or minimum value of the vortex-free case allows you to match up all of the remaining angular momenta with the angular momenta of the vortex case in such a way that the resulting energy difference converges as you increase the amount of angular momenta you consider.

We also need to consider the mean-field decoupling term. When we perform the mean-field decoupling, we get a term of the form $\langle c^\dagger_{k\uparrow} c^\dagger_{-k\downarrow}\rangle\langle c_{-k'\downarrow} c_{k'\uparrow}\rangle$. This term has been analyzed in appendix C, and shown to be equal to

$$E_\Delta = \frac{2}{g}\int_0^R \mathrm{d}r|\Delta(r)|^2 r \tag{75}$$

In practice, we simply take the integral up to $\frac{R}{3}$, as after that both the vortex and vortex-free case has the same value, and as such the integral out there is irrelevant. We now compute E_{vb} for a range of m_0, and plot them in figure 11. We see that an impurity does in fact stabilize a vortex, which confirms one of the key results from [3]. For the parameters we used, which has $\lambda_0 = 6.6$ meV, you need $m_0 = 7.2$ meV to stabilize the vortex, which is slightly higher than in [3], but not unreasonably so. This spontaneous vortex is called a quantum anomalous vortex, and we also see that a vortex formed due to an external field will still form around the impurity, since the impurity lowers the energy of the vortex.

4.1 Helical band

We now turn our attention to a new case: Self-consistent solutions with a helical band. If we start by considering the situation with no coupling to the magnetic ion, we see that our result is very similar to that with a parabolic band. The most interesting difference is that we no longer have spin-symmetry in the density of states, and that our angular momenta eigenvalues are shifted by $\frac{1}{2}$ compared to the parabolic band. Looking at the vortex case, the CdGM states are clearly visible on the DOS, as can be seen on figure 12. If we look at the spin-polarized DOS, we see that there is a zero-energy mode present with spin-up. We can check whether this is a Majorana state by plotting u_σ and v_σ for this state. Doing that reveals that it is indeed a Majorana state. The fact that we get a Majorana state in the vortex of a helical band is well-known

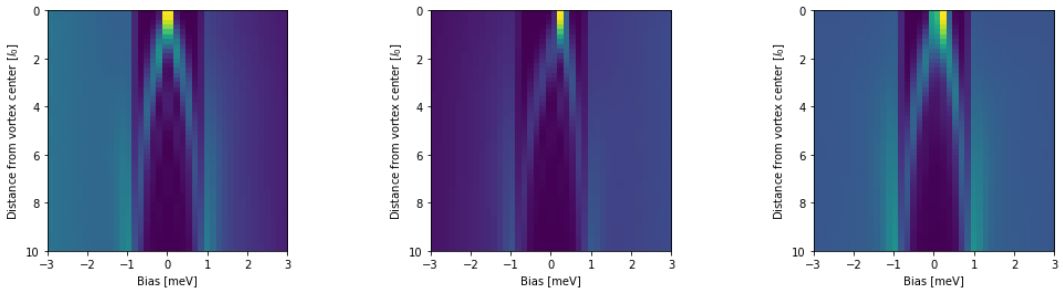

(a) Spin-up (b) Spin-down (c) Total

Figure 12: Local DOS near a vortex in a helical band.

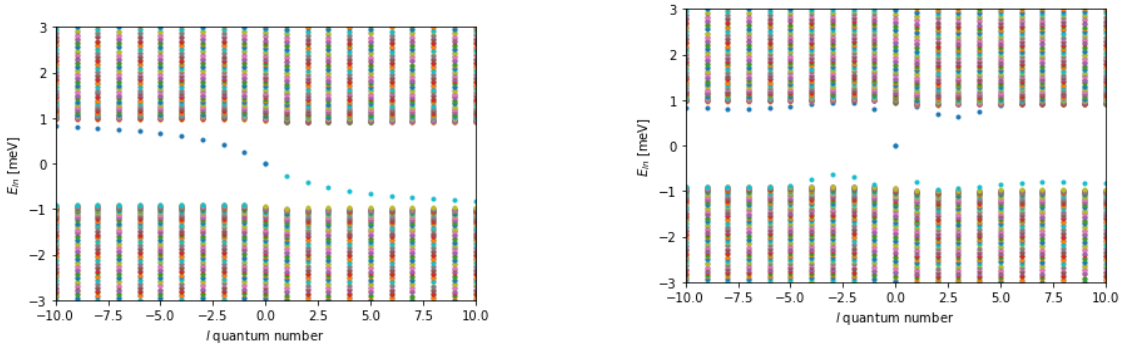

(a) Energy spectrum of a vortex in a helical band.

(b) Energy spectrum of a vortex at a magnetic impurity with $m_0 = 5$ meV in a helical band.

Figure 13: Energy spectra for a helical band vortex.

from analytical results [7][11]. The prominent spin-down state at $r = 0$ is also predicted by analytical results, and is offset from the Majorana state due to the breaking of spin-symmetry in the Rashba Hamiltonian[11]. When we introduce the magnetic impurity, we see that the CdGM states get pushed out of the gap. This is both seen on the DOS in figure 14 and the spectra in figure 13. This doesn't apply to the Majorana state, which stays at zero energy and is thus isolated from the other states. The very prominent state next to the Majorana state is also supressed. These results are comparable to those found in [3] for a situation where the gap was induced by the underlying bulk material, as opposed to this situation where the gap is generated in the surface. We note that the magnitude of λ_0 doesn't have a strong effect on the system.

If we consider an impurity without an associated vortex, the DOS looks markedly different. We see that the in-gap states are not zero-energy. While it might be possible to tune the in-gap states to be zero-energy, we also see that the spin-polarization is different. The sub-gap states at $r = 0$ for spin-up and spin-down correspond to $\mu = \pm\frac{1}{2}$. The symmetry of these states means that a zero-energy state wouldn't be spin-up polarized like a Majorana zero mode, and as such they would have different properties.

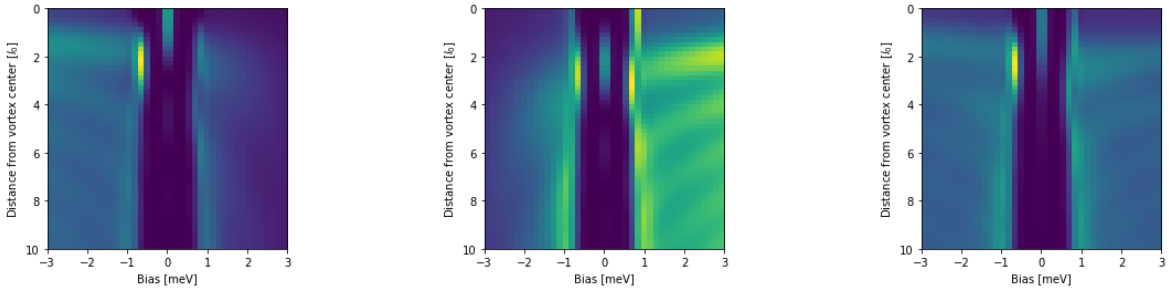

(a) Spin-up (b) Spin-down (c) Total

Figure 14: Local DOS near a vortex in a helical band, with a magnetic impurity with $m_0 = 5$ meV and $\lambda_0 = 2$ meV.

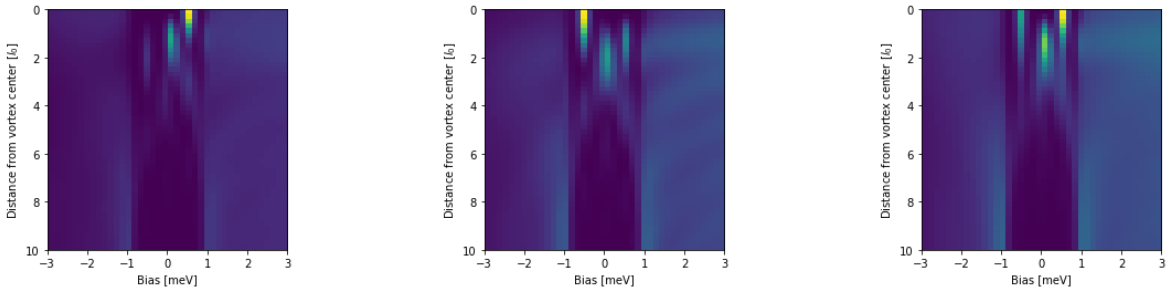

(a) Spin-up (b) Spin-down (c) Total

Figure 15: Local DOS near a magnetic impurity in a helical band, with $m_0 = 5$ meV and $\lambda_0 = 2$ meV.

5 Conclusion

In this thesis, we've used the BdG equations to analyze the behaviour of a vortex in a type II superconductor in the presence of a magnetic impurity. By writing these equations in terms of Bessel functions, we have been able to write a program that solves them for a number of different cases. We've primarily used this program to analyze the same cases as [3], as well as to solve the BdG equations self-consistently for a helical band. Our analysis was largely in agreement with [3], and furthermore found that our method of solving the BdG equations self-consistently for a helical band yields a qualitatively similar result to solving them with a Δ induced by the underlying bulk of the material. We also found that the solutions for the helical band do not yield Majorana-like modes without the presence of a vortex.

The major product of this thesis is a program that can solve these equations. This program can easily be rewritten to consider a number of interesting cases, including different forms of the electron Hamiltonians, and different electron-impurity interactions. These studies would provide even more insight into the problem, and allow us to analyze more complicated setups as long as they follow the basic symmetries that we used to do the Bessel decomposition.

References

[1] Brian Møller Andersen, Lecture notes from Condensed Matter Physics 2, Niels Bohr Institute, 2017

[2] James F. Annett, Superconductivity, superfluids and condensates, Oxford University Press, 2004

[3] Kun Jiang, Xi Dai & Ziqiang Wang, Quantum anomalous vortex and Majorana zero mode in iron-based superconductor Fe(Te,Se), Physical Review X **9**, 2019

[4] Pierre G. de Gennes, Superconductivity of Metals and Alloys, CRC press, 2018

[5] F. Gygi & M. Schlüter, Self-consistent electronic structure of a vortex line in a type II superconductor, Physical Review B vol. 43, 1990

[6] H. Deng, N. Bonesteel & P. Schlottmann, Bound fermion states in pinned vortices in the surface states of a superconducting topological insulator, Journal of Physics: Condensed Matter **33**

[7] Adam C. Durst, Scattering state of a vortex in the proximity-induced superconducting state at the interface of a topological insulator and a superconductor, Physical Review B **93**, 2016

[8] Kun Jiang, Xi Dai & Ziqiang Wang, Supplemental material for Quantum anomalous vortex and Majorana zero mode in iron-based superconductor Fe(Te,Se), 2019

[9] Hano Omar Mohammad Sura, Notes & personal communication, 2021

[10] Christin Edblom, Numerical Studies of Vortex Core States in Type II Superconductors, Masters thesis, Umeå University, 2012

[11] P. Schlottmann, Local density of states in a vortex at the surface of a topological insulator in a magnetic field, The European Physical Journal B, 2021

[12] A. Kreisel, P. J. Hirschfeld & B. M. Andersen, On the remarkable superconductivity of FeSe and its close cousins, Symmetry, 2020

A Kinetic term

We want to compute the kinetic term for the Bessel decomposition of the helical band. To do this, we consider the generic form of this term:

$$V_{ij} = \hbar v_D \int_0^R \mathrm{d}r r \phi_{il}(r)(\partial_r \pm \frac{l'}{r})\phi_{jl'}(r) \tag{76}$$

We write this in terms of Bessel functions:

$$V_{ij} = \frac{2\hbar v_D}{R^2 J_{l+1}(\beta_{li}) J_{l'+1}(\beta_{l'i})} \int_0^R \mathrm{d}r J_l(\frac{\beta l i}{R} r)(\partial_r \pm \frac{l'}{r}) J_{l'}(\frac{\beta l' j}{R} r)$$

For the following calculations, we use a number of relations for Bessel functions:

$$\begin{aligned} J_l'(x) \pm \frac{l}{x} J_l(x) &= \pm J_{l\mp 1}(x) \\ \int_a^b \mathrm{d}x x J_l(\alpha x) J_l(\beta x) &= \frac{1}{\alpha^2 - \beta^2}[\beta x J_l(\alpha x) J_l'(\beta x) - \alpha x J_l(\beta x) J_l'(\alpha x)]_a^b \\ J_{l-1}(x) + J_{l+1}(x) &= \frac{2l}{x} J_l(x) \end{aligned} \tag{77}$$

Where $J_l'(x)$ is the derivative of the Bessel function. We thus get:

$$\begin{aligned}\frac{2\hbar v_D}{R^2 J_{l+1}(\beta_{li}) J_{l'+1}(\beta_{l'i})} \int_0^R \mathrm{d}r J_l(\frac{\beta_{li}}{R} r)(\partial_r \pm \frac{l'}{r}) J_{l'}(\frac{\beta_{l'j}}{R} r) = \\ \frac{\pm 2\hbar v_D}{R^2 J_{l+1}(\beta_{li}) J_{l'+1}(\beta_{l'i})} \frac{\beta_{l'j}}{R} \int_0^R \mathrm{d}r J_l(\frac{\beta_{li}}{R} r)(\pm J_{l'\mp 1}(\frac{\beta_{l'j}}{R} r)) = \\ \frac{\pm 2\hbar v_D}{R^2 J_{l'+1}(\beta_{l'i})} \frac{\beta_{l'j}}{R} \frac{R^2}{\beta_{li}^2 - \beta_{l'j}^2} (-\beta_{li} J_l(\beta_{l'j}) J_l'(\beta_{li})) = \\ -\frac{\hbar v_D R}{2} \frac{\beta_{li}\beta_{l'j}}{\beta_{li}^2 - \beta_{l'j}^2}\end{aligned} \tag{78}$$

Note that there is an error in [8], where they have the wrong sign.

B BdG equation matrices

To calculate the energies and Bessel coefficients in the BdG equations, we use matrices. These matrices are a combination of the matrix found through Bessel decomposition and the extra terms from the impurity. The full matrices are provided here:
For a parabolic band, with $\nu = 0$:

$$\begin{pmatrix} (T - L - M - \Lambda)_l & 0 & \Delta_l & 0 \\ 0 & (T - L + M + \Lambda)_l & 0 & \Delta_l \\ \Delta_l^T & 0 & -(T + L + M - \Lambda)_l & 0 \\ 0 & \Delta_l^T & 0 & -(T + L - M + \Lambda)_l \end{pmatrix} \tag{79}$$

For a parabolic band with $\nu = 1$

$$\begin{pmatrix} (T - L - M - \Lambda)_{\mu^+} & 0 & \Delta_{\mu^+,\mu^-} & 0 \\ 0 & (T - L + M + \Lambda)_{\mu^+} & 0 & \Delta_{\mu^+,\mu^-} \\ \Delta_{\mu^+,\mu^-}^T & 0 & -(T + L + M - \Lambda)_{\mu^-} & 0 \\ 0 & \Delta_{\mu^+,\mu^-}^T & 0 & -(T + L - M + \Lambda)_{\mu^-} \end{pmatrix} \tag{80}$$

For a helical band with $\nu = 0$:

$$\begin{pmatrix} -(L + M + \Lambda)_{\mu^-} + \varepsilon_F & V_{\mu^-,\mu^+} & \Delta_{\mu^-} & 0 \\ V_{\mu^-,\mu^+}^T & -(L - M - \Lambda)_{\mu^+} + \varepsilon_F & 0 & \Delta_{\mu^+} \\ \Delta_{\mu^-}^T & 0 & -(L + M - \Lambda)_{\mu^-} + \varepsilon_F & V_{\mu^-,\mu^+} \\ 0 & \Delta_{\mu^+}^T & V_{\mu^-,\mu^+}^T & -(L - M + \Lambda)_{\mu^+} + \varepsilon_F \end{pmatrix} \tag{81}$$

And for a helical band with $\nu = 1$

$$\begin{pmatrix} -(L + M + \Lambda)_l + \varepsilon_F & V_{l,l+1} & \Delta_{l,l-1} & 0 \\ V_{l,l+1}^T & -(L - M - \Lambda)_{l+1} + \varepsilon_F & 0 & \Delta_{l,l+1} \\ \Delta_{l,l-1}^T & 0 & -(L + M - \Lambda)_{l-1} + \varepsilon_F & V_{l-1,l} \\ 0 & \Delta_{l+1,l}^T & V_{l-1,l}^T & -(L - M + \Lambda)_l + \varepsilon_F \end{pmatrix} \tag{82}$$

With all terms defined as in the text.

C Energy terms

When deriving the BdG equations, we get a number of energy terms that we don't include in the equations. These terms can potentially matter when we calculate the energy difference of different setups. As such, we need to take them into account. The first extra term is the one that we get from the mean field decoupling: $\int \mathrm{d}\boldsymbol{r}\langle\psi_\uparrow(\boldsymbol{r})^\dagger c_\downarrow(\boldsymbol{r})^\dagger\rangle\langle c_\downarrow(\boldsymbol{r})c_\uparrow(\boldsymbol{r})\rangle$. This can be rewritten as $\int \mathrm{d}\boldsymbol{r}\frac{2|\Delta(\boldsymbol{r})|^2}{g}$. Using rotational symmetry of our setup, this can simply be rewritten as:

$$\frac{4\pi}{g}\int_0^R \mathrm{d}r|\Delta(r)|^2 r \tag{83}$$

There is, however, a very subtle catch here. We calculate Δ in terms of $u(r)$ and $v(r)$, so we want those to be correct. To get the correct $u(r)$ and $v(r)$, we use the fact that our Bogoliubov transformation is unitary, so

$$\int \mathrm{d}\boldsymbol{r}|u(\boldsymbol{r})|^2 + |v(\boldsymbol{r})|^2 = 1 \tag{84}$$

Using our symmetry here, this can be rewritten as

$$2\pi\int \mathrm{d}r|u(r)|^2 + |v(r)|^2 = 1 \rightarrow \int \mathrm{d}r|u(r)|^2 + |v(r)|^2 = \frac{1}{2\pi} \tag{85}$$

This is not the normalization we've been using, however. We've instead simply normalized it such that the right-hand integral is equal to 1. To correct for our faulty normalization, we can simply divide this energy term by 2π, so we get the final energy term:

$$E_\Delta = \frac{2}{g}\int_0^R \mathrm{d}\boldsymbol{r}|\Delta(r)|^2 r \tag{86}$$